Dawn and dusk sector comparisons of small-scale irregularities, convection, and particle precipitation in the high-latitude ionosphere

Raymond A. Greenwald, Simon G. Shepherd,[1] Thomas S. Sotirelis,
J. Michael Ruohoniemi, and Robin J. Barnes
Applied Physics Laboratory, Johns Hopkins University, Laurel, Maryland, USA

Received 7 June 2001; revised 31 October 2001; accepted 4 December 2001; published 19 September 2002.

[1] Small-scale ionospheric irregularities and auroral precipitation are common features of the auroral ionosphere, but their spatial association has not been examined on global scales. In this paper, we compare electron and ion precipitation from individual passes of the Defense Meteorological Satellite Program (DMSP) spacecraft with concurrent observations of ionospheric irregularities and plasma convection from the Northern Hemisphere component of the Super Dual Auroral Radar Network (SuperDARN). Because of the nature of the DMSP orbits and the spatial resolution of the SuperDARN measurements these comparisons have been limited to the dusk and postdawn sectors and spatial dimensions greater than ~100 km. We have found that the SuperDARN radars generally observe ionospheric irregularities over a greater latitudinal extent than the DMSP satellites observe particle precipitation. Specifically, ionospheric irregularities are observed both equatorward and poleward of the convection reversal boundary (CRB) in the dawn and dusk sectors, whereas particle precipitation is only observed equatorward of the CRB. Under conditions where the radars can detect the true equatorward boundary of the irregularities, they are observed to extend equatorward of the particle precipitation. Both irregularities and particle precipitation expand equatorward with increasing geomagnetic activity, and there is evidence that precipitation regions with higher energy flux are associated with regions of stronger sunward convection. These results suggest that SuperDARN can provide a coarse determination of the auroral-oval position that will complement measurements with optics and particle detectors. More importantly, they demonstrate the spatial relationships between precipitation, electric fields, and ionospheric irregularities that result from the electrical coupling between the magnetosphere and ionosphere and the dependence of ionospheric plasma instabilities on the ionospheric electric field and precipitation-induced electron-density gradients. *INDEX TERMS:* 2760 Magnetospheric Physics: Plasma convection; 2407 Ionosphere: Auroral ionosphere (2704); 2463 Ionosphere: Plasma convection; 2455 Ionosphere: Particle precipitation; 2439 Ionosphere: Ionospheric irregularities; *KEYWORDS:* irregularities, convection, precipitation, ionosphere, magnetosphere

Citation: Greenwald, R. A., S. G. Shepherd, T. S. Sotirelis, J. M. Ruohoniemi, and R. J. Barnes, Dawn and dusk sector comparisons of small-scale irregularities, convection, and particle precipitation in the high-latitude ionosphere, *J. Geophys. Res.*, *107*(A9), 1241, doi:10.1029/2001JA000158, 2002.

1. Introduction

[2] Over the past 7 years, the SuperDARN radar network has been used increasingly as a tool to image the global-scale structure and dynamics of high-latitude plasma convection and electric fields. The radars provide this information through detection of Bragg backscattered signals from field-aligned electron density irregularities. These irregularities have scale sizes of 7.5–19 m commensurate with the 8–20 MHz operating frequency of the radars. At ranges of less than ~600 km from each radar site, the signals are typically backscattered by *E* region irregularities produced by plasma instabilities in the auroral electrojets [e.g., *Hanuise et al.*, 1981]. At greater ranges and over most of the fields of view of the radars, the backscattered signals are caused by *F* region irregularities resulting from plasma turbulence most often attributed to a gradient instability (see *Reid* [1968] and review by *Fejer and Kelley* [1980]). With typical electron-density gradients found in the auroral ionosphere, this instability is linearly unstable at wavelengths greater than 100 m. However, once the plasma becomes linearly unstable within some wavelength range and direction of propagation, plasma turbulence quickly leads to the growth of unstable modes at smaller wave-

[1]Now at Thayer School of Engineering, Dartmouth College, Hanover, New Hampshire, USA.

0148-0227/02/2001JA000158$09.00

lengths and in propagation directions that are essentially isotropic in the plane perpendicular to the magnetic field.

[3] Examination of the *F* region gradient drift instability mechanism suggests that irregularities should be generated in those regions of the high-latitude ionosphere where plasma convection is aligned with naturally occurring electron density gradients. These conditions occur near the dawn and dusk terminators, in the cusp, and in the auroral oval. Irregularities produced in these regions will be transported by high-latitude electric fields to other regions of space that are not inherently unstable [*Fejer and Kelley*, 1980]. While the irregularities will decay, if a source of free energy is not available, the rate of decay can be slow, particularly if the electrical conductance in the underlying *E* region is low. Thus *F* region irregularities produced in restricted regions of the high-latitude ionosphere may circulate to fill large areas within the high-latitude polar region. These general arguments are consistent with observations by *Kivanc and Heelis* [1998] who reported a statistical study of DE 2 drift meter data showing strong kilometer-scale density irregularities throughout the polar cap for winter conditions under both northward and southward IMF.

[4] The actual spatial distribution of small-scale high-latitude ionospheric irregularities is something that has not been thoroughly investigated. *Bates et al.* [1973] postulated that they are collocated with the auroral oval. This conjecture was based upon his observations with a rotating oblique ionosonde located at Resolute Bay, Canada, that showed an instantaneous ring-like distribution of scattering sources about the magnetic pole. *Ruohoniemi and Greenwald* [1997] and *Milan et al.* [1997] presented statistical studies of the occurrence of high-latitude *F* region backscatter and found that the backscattering irregularities maximized over a broad region that was roughly coincident with the statistical auroral oval.

[5] In this paper, we extend this earlier work by comparing the location of ionospheric irregularities observed with the SuperDARN radar network [*Greenwald et al.*, 1995] with the location of precipitating particles observed with the Defense Meteorological Satellite Program (DMSP) satellites. DMSP spacecraft were selected because they are standard low Earth-orbit monitors that can detect precipitating particles to levels below that which produce detectable auroral luminosity. The spacecraft are in Sun-synchronous orbits that limit their local time coverage, but allow some movement in magnetic local time as a consequence of the offset of the Earth's dipole. The combination of SuperDARN radar locations and DMSP orbit planes determined the magnetic local time coverage of this study. In general, it was rather good throughout the afternoon and evening sectors, but limited on the dawn side to postdawn hours.

[6] The study utilizes several days of observations in 1997 and 1999. The 1997 data were selected from periods for which there were relatively stable interplanetary magnetic field (IMF) conditions, extensive radar backscatter observed with the Northern Hemisphere component of SuperDARN, and particle observations from four DMSP spacecraft (F11, F12, F13, and F14). While we present only a single example from the 1997 data set, the example is characteristic of several days of observations that revealed a close macroscale spatial relationship between electron and/or ion precipitation and *E* and/or *F* region irregularities. This study included an analysis of the Doppler properties of the backscattered radar signals and revealed that the auroral precipitation was associated with regions of sunward moving ionospheric irregularities.

[7] During the 1997–1999 time frame, the SuperDARN radars had more limited spatial coverage than they currently do [see *Shepherd and Ruohoniemi*, 2000] and it was impossible to obtain concurrent radar observations in the midmorning and midafternoon/evening local time sectors. In addition, the four DMSP spacecraft generally did not pass over the Northern Hemisphere polar region at the same time, which again limited the concurrent global coverage. These factors required us to integrate the SuperDARN data for periods approaching one hour in order to compare the SuperDARN measurements with those from most or all of the DMSP spacecraft. To improve the temporal comparison, we have adopted a different, more quantitative approach with the 1999 data set. Specifically, the DMSP spacecraft are situated in two orbital planes that are roughly aligned with the dawn-dusk and premidnight-prenoon meridians. The data along these orbital planes have been grouped into three distinct magnetic local time (MLT) sectors: 0600–0900 MLT, 1700–1900 MLT, and 2000–2100 MLT. Equatorward of the convection reversal boundary (CRB), each of these sectors is associated with sunward convecting plasma and each of the SuperDARN radars passes through each of the local time bins during specific parts of the UT day. We have compared the data from 36 satellite passes with concurrent radar observations along the satellite path. These passages correspond to a fairly wide range of geophysical conditions and each is identified with one of the selected local time bins. The analysis is not carried out in a statistical manner, but rather as a composite view of a large number of individual events. This allows us to display the variability of the individual comparisons, while at the same time revealing the underlying characteristic behavior. We again observe a consistent close spatial overlap between regions of particle precipitation and regions of sunward convecting irregularities over a wide range of geomagnetic conditions. In this paper, we present these results and discuss them in terms of the large-scale current systems that electrically couple the magnetosphere with the high-latitude ionosphere and the small-scale plasma instability processes that lead to the formation of ionospheric irregularities.

2. Instrumentation

[8] The data in this paper were obtained with the SuperDARN radar network and the previously identified DMSP spacecraft. From 1997 to 1999, there were six operating radars in the Northern Hemisphere portion of the SuperDARN network and five radars in the South. In the current paper, we only use the Northern Hemisphere radars, which extend from Saskatoon, Saskatchewan, eastward across Canada and Iceland to Hankasalmi, Finland (see Figure 1). Typically, each radar scans through 16-beam directions every 2 min. Each beam is associated with an azimuthal step of 3.2°, yielding a total radar azimuth scan of 51° [*Greenwald et al.*, 1995].

[9] The SuperDARN radars transmit a complex sequence of pulses that, when backscattered by ionospheric irregu-

Figure 1. Plan view of Northern Hemisphere SuperDARN radars for the time interval of this study.

larities, received and analyzed, yield a complex autocorrelation function (ACF) of the backscattered signal as a function of range. These ACFs are further processed to determine the Doppler velocity of the backscattered returns as a function of range from the radar and the Doppler spectral width. We only consider the first of these quantities in this paper.

[10] The Doppler velocity data from the radars are further processed using a spherical harmonic analysis technique described by *Ruohoniemi and Baker* [1998] and *Shepherd and Ruohoniemi* [2000] to obtain the electrical potential pattern that drives high-latitude plasma circulation. While these patterns are typically obtained every 2 min, it is possible to average the Doppler data from multiple radar scans, particularly if IMF conditions are stationary. An example of the convection patterns that were obtained during this study is shown in the top plot of Figure 2. The data are from 16 December 1977 for the interval from 2250–2300 UT. These data are from an extended 5-hour interval of quasi-stationary negative B_z and B_y. The convection patterns obtained during this interval are generally similar to the one shown here.

[11] In Figure 2 the solid black curves represent the contours of the negative, dusk potential cell, while the dashed curves represent the contours of the positive, morning cell. The electric potential associated with every second contour is identified and the contour spacing is 6 kV. The green contour is the estimated equatorward boundary of high-latitude convection. It has a shape determined by *Heppner and Maynard* [1987] and is dynamically adjusted to the equatorward boundary of significant irregularity drift velocities [*Shepherd and Ruohoniemi*, 2000]. The top plot also displays the convection velocities that are derived from the analysis process. Each velocity is indicated by a dot representing the location of the measurement and a line extending from the dot and representing the direction and magnitude of the fitted velocity vector. The magnitude of the velocity vector is also indicated by the color. These vectors are plotted at each location in the analysis grid where Doppler data were available from one or more of the SuperDARN radars. One can clearly see that data are only available from the ~12 hour MLT sector where SuperDARN radars were in operation. In this case, the coverage extends over the dusk cell and into the dawn cell near midnight. A sparse distribution of model vectors has been used to stabilize the solution in areas where no observations were available. Vectors are not plotted in these regions so as to caution the reader that the solutions there are not strongly constrained by measurements.

[12] Each DMSP spacecraft is in a Sun-synchronous circular orbit at an altitude of 840 km. One of the spacecraft has a near dawn-dusk orbit (F13), two have 1030–2130

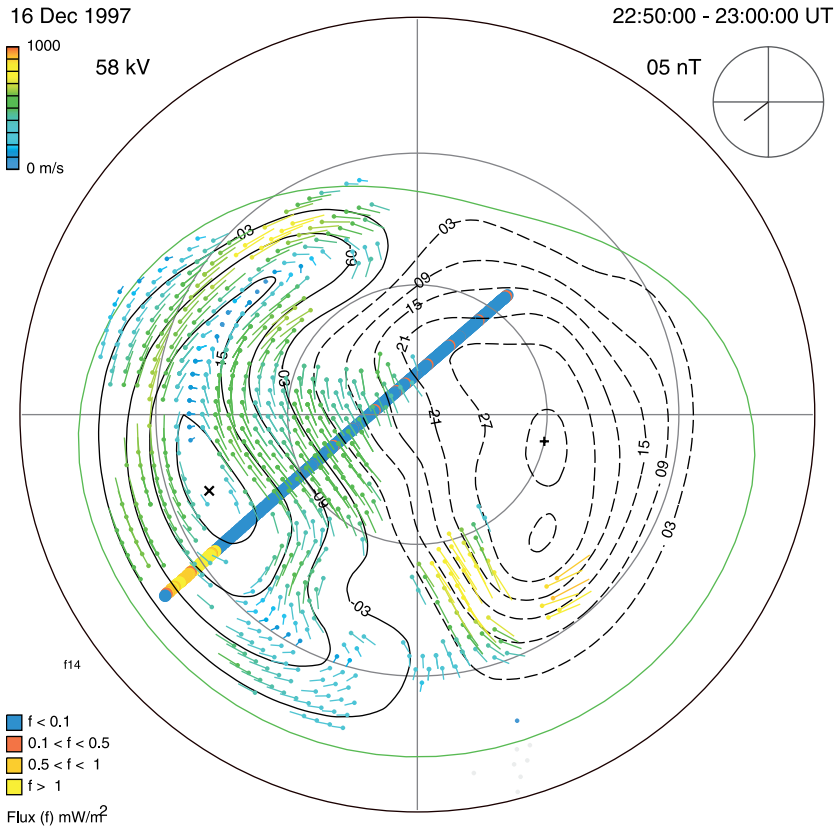
16 Dec 1997
22:50:00 - 23:00:00 UT
1000
58 kV
05 nT
0 m/s
f14
f < 0.1
0.1 < f < 0.5
0.5 < f < 1
f > 1
Flux (f) mW/m2

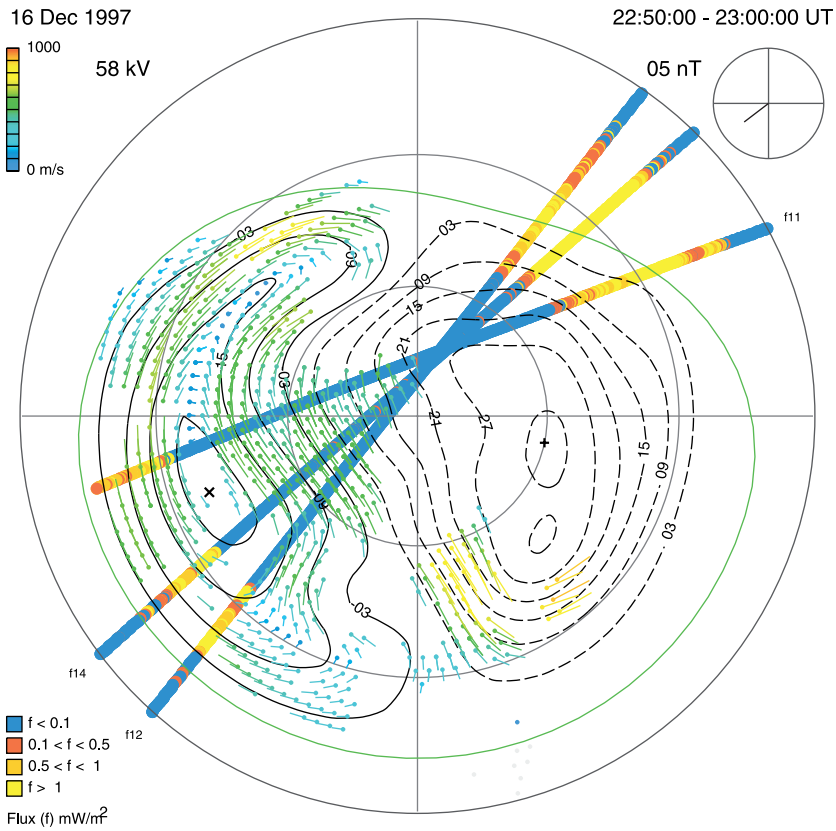
16 Dec 1997
22:50:00 - 23:00:00 UT
1000
58 kV
05 nT
0 m/s
f11
f14
f12
f < 0.1
0.1 < f < 0.5
0.5 < f < 1
f > 1
Flux (f) mW/m2

local time orbits (F12 and F14), and one has a 0730–1930 local time orbit (F11). Each spacecraft instrument package includes a set of electrostatic sensors for detecting precipitating ions and electrons in the energy range from 50 eV to 30 keV. The colored stripe in the upper plot of Figure 2 represents the integrated and summed energy flux of precipitating electrons and ions observed along the spacecraft trajectory over 1 s intervals (~7 km). The data have been binned into one of four levels of precipitating energy flux as indicated by the color. The lowest level, <0.1 mW/m^2, is indicated by dark blue and corresponds to virtually no precipitation. The next level, 0.1–0.5 mW/m^2, is indicated by red and corresponds to sub-visual to weak aurora. The third level, 0.5–1.0 mW/m^2 is indicated by orange and corresponds to moderate aurora and the final level, >1 mW/m^2, is indicated by yellow and corresponds to strong aurora. The orbit segment shown, has a length of 4200 km and represents the distance traversed by DMSP F14 during a 10-min interval (equivalent to five scans of the SuperDARN radars).

[13] Since the orbits of the spacecraft are asynchronous with each spacecraft only moving 4200 km during the 10-min integration, it is uncommon for more than one or two DMSP spacecraft to pass over the Northern Hemisphere polar region at any selected time. For this reason, we have extended the time for inclusion of DMSP data to ±25 min about the mid time of the SuperDARN integration interval that was used, 2255 UT on 16 December 1997. This enables us to compare the SuperDARN measurements with data from up to four satellites. Using a broader DMSP acceptance interval is acceptable because of the previously noted stability of both the IMF and the observed SuperDARN convection patterns. In the example shown in the lower plot of Figure 2, three DMSP spacecraft have passed over the Northern Hemisphere polar region during the 50-min acceptance interval. In each case, the dusk sector particle precipitation is collocated with the latitudinal region of largest sunward convection. Indeed, the latitudinal intervals of intense particle precipitation are bounded on the equatorward side by the zero-potential boundary and on the poleward side by the CRB. In contrast, on the dawnside, all three spacecraft show precipitation extending well equatorward of the zero-potential boundary as indicated by the closed green contour. Note, however, that the dawnside boundary has not been determined by observations, so this offset may be spurious.

3. Multievent Analyses

[14] Since the total longitudinal coverage of the combined fields of view of the SuperDARN radars is limited, it is impossible to produce simultaneous overlapping coverage of SuperDARN and DMSP observations in both the dawn and dusk convection cells. For this reason, we have compared these two data sets within limited local time sectors for a number of days and under varying levels of geomagnetic activity.

[15] Figure 3 displays an extensive comparison of 20 passes of DMSP spacecraft in the 1700–1900 MLT sector. The ordinate axis in Figure 3 is invariant latitude, and the tic marks along the abscissa are associated with each of the events. For each event the top row of numbers represents month and day, the second row represents the UT start time of the 6-min SuperDARN analysis interval with which the DMSP data are compared, and the bottom number represents the *Kp* index at that time. The events have been ordered in terms of increasing levels of activity as determined by the equatorward edge of the ion precipitation boundary observed by DMSP. The light-blue and dark-blue bands identify the latitude range over which sunward moving ionospheric irregularities were observed. Antisunward moving irregularities located poleward of the CRB have not been displayed. The light-blue bands represent irregularity regions in which the convection velocity derived from the SuperDARN convection analysis is less than half of the peak sunward convection velocity determined along the DMSP trajectory for that pass, whereas the dark-blue band is where it is greater than 50% of the peak velocity. Since each of the peak-velocity determinations is made specifically for a given DMSP overflight, it is entirely possible that velocities in the light-blue portion of one determination are greater than velocities in the dark-blue portion of another determination. The color discrimination is used only to localize where the largest velocities were observed on a given pass.

[16] In the present example, the results may be related to the 1700–1900 MLT segment of Figure 2, only they cover a much wider range of activity levels. The dark line denoted as HMB represents the Heppner-Maynard low-latitude boundary of ionospheric convection (zero potential boundary). This boundary is derived from the complete set of Northern Hemisphere SuperDARN observations. SBLL is the low-latitude boundary of ionospheric scatter in the local time sector of the DMSP pass, HVLL and HVUL are the low- and high-latitude boundaries of higher-velocity ionospheric flow within the local time sector and CRB is the latitude of the convection reversal boundary.

[17] There are several features to note in Figure 3. Most importantly, particle precipitation is much more highly structured and almost exclusively associated with regions of sunward moving irregularities. The difference in structure is a consequence of the different spatial resolution offered by SuperDARN and DMSP and by the smoothing associated with the SuperDARN convection analysis. The spatial

Figure 2. (opposite) (top) Polar plot of high-latitude convection pattern in geomagnetic coordinates as derived from SuperDARN radar observations. Noon is at the top, and dusk is to the left. Flow vectors are plotted at grid locations where at least one radar measurement was obtained. The superposed stripe represents the total precipitating electron and ion energy flux observed along the orbit of the DMSP F12 spacecraft during the integration interval. Note that in the dusk sector the most intense precipitating energy flux is collocated with strong sunward plasma convection. (bottom) Same as the top plot but with satellite data from three spacecraft for ±25 min about the mid time of the radar integration. Again, note the overlap of strong precipitation and strong sunward flows in the dusk sector. The morning sector precipitation appears to extend equatorward of the dawn convection cell; however, this is unconfirmed by radar observations.

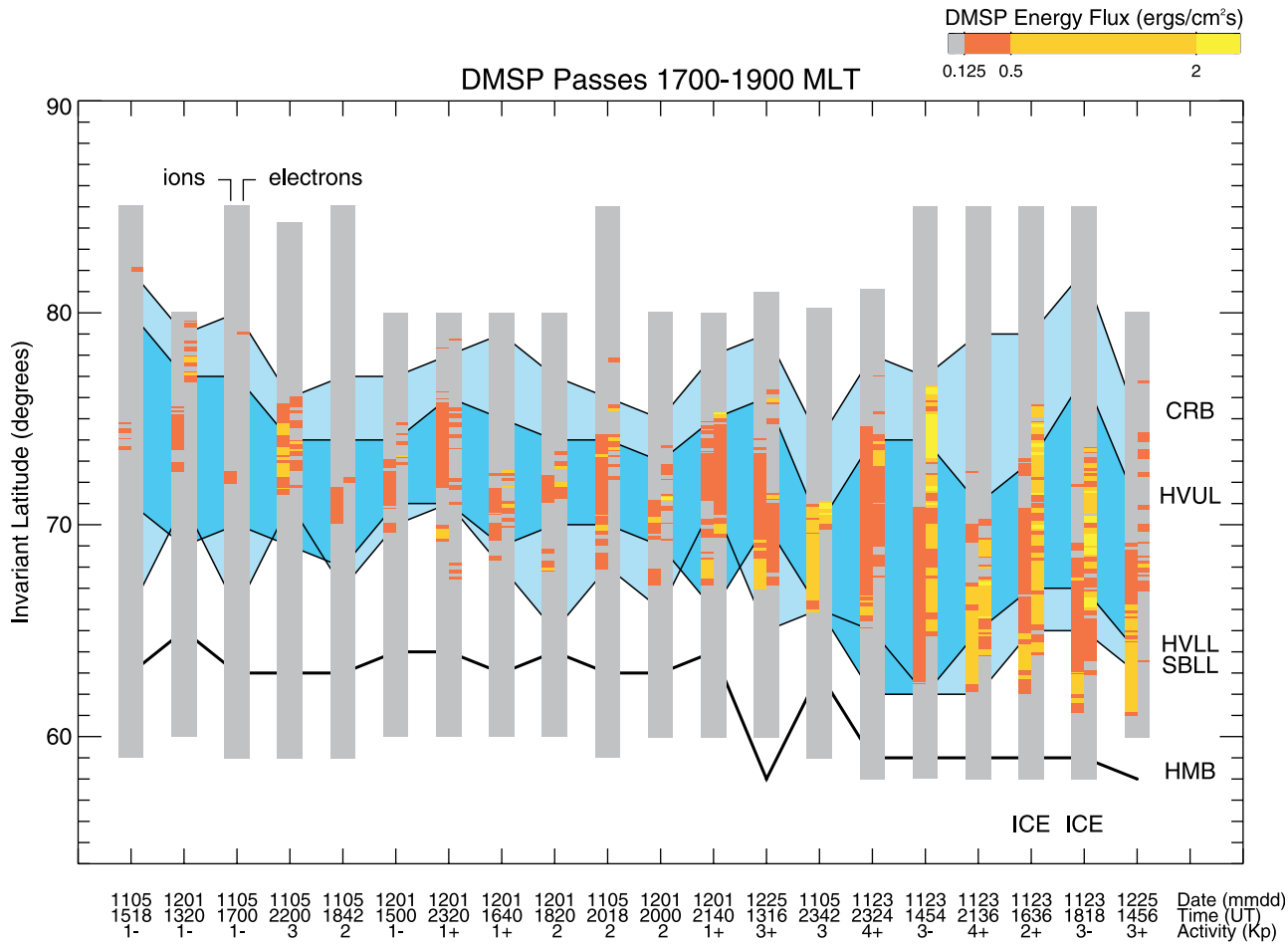

Figure 3. Comparison of DMSP observations of precipitating electrons and ions with SuperDARN observations of ionospheric irregularities and convection for the 1700–1900 MLT sector. For each of these events, there was extensive backscatter from ionospheric irregularities along the spacecraft trajectory. The vertical colored stripes represent DMSP observations of precipitating ion and electron energy flux. HMB represents the Heppner-Maynard low-latitude boundary of ionospheric convection as derived from all Northern Hemisphere SuperDARN observations, SBLL is the low-latitude boundary of ionospheric scatter in the local time sector of the DMSP pass, HVLL and HVUL are the low- and high-latitude boundaries, respectively, of high-velocity ionospheric flow (greater than 50% of the maximum velocity) within the local time sector, and CRB is the latitude of the convection reversal boundary derived from SuperDARN measurements. All comparisons are from 1999. The abscissa indicates from top to bottom: month and day of observation, UT time of observation based on initial time of SuperDARN three-scan average, and the *Kp* index. The comparisons have been ordered from low to high activity as determined by the equatorward boundary of ion precipitation. The passes indicated by ICE, occur when the Iceland radars are in the 1700–1900 MLT sector. These radars are located at $\Lambda = 65°$ and might not detect the true equatorward boundary of the backscatter.

coherence remains intact as both the irregularities and the precipitation expand equatorward with increasing geomagnetic activity. It also appears that greater energy fluxes of precipitating particles are concentrated in regions of higher velocity flow. The few exceptions to these general relationships occur when the oval is very expanded and/or the 1700–1900 MLT SuperDARN radars are located in Iceland (ICE on Figure 3). Since these radars are located at $\Lambda = 65°$, they are unable to detect the true equatorward boundary of ionospheric irregularities even for a moderately expanded auroral oval.

[18] Figure 4 shows a similar comparison of DMSP and SuperDARN observations for the 2000–2100 MLT sector. In this sector it is more difficult to perform such comparisons because the auroral oval extends more equatorward near midnight, while the radars remain at fixed locations. We find that when the Iceland radars are in this local time sector (2030 UT and 2210 UT), DMSP particle precipitation is often observed equatorward of where the radars make measurements. The same situation may have occurred for the 2340 UT pass on December 1, 1999. At that time, Greenland was in the local time sector of interest and neither the Stokkseyri radar (Iceland) nor the Goose Bay radar (located in Canada at $\Lambda = 63°$) was able to detect backscatter to the lowest latitudes that precipitation was observed. In contrast, the Hankasalmi radar in Finland is

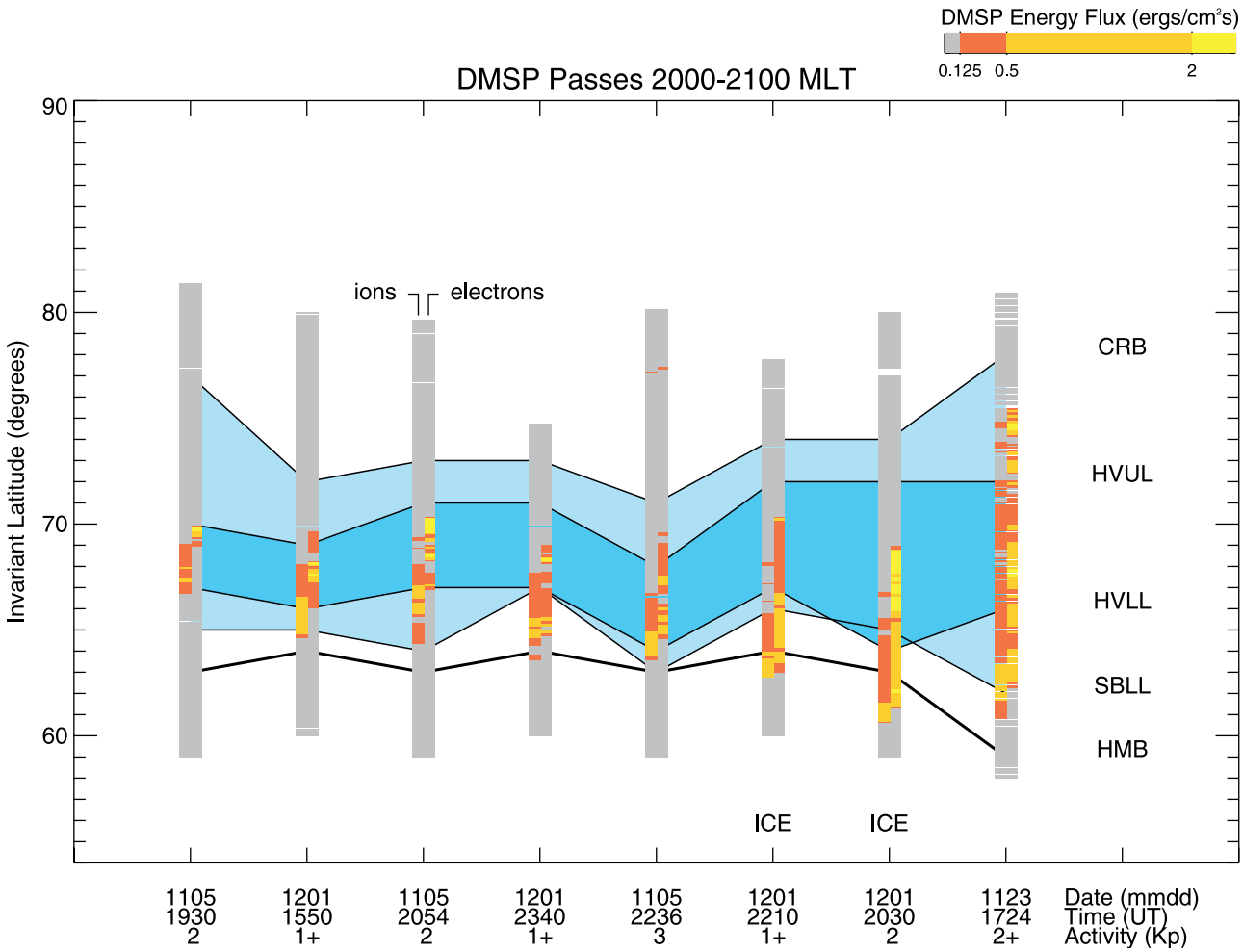

Figure 4. Comparison of DMSP observations of precipitating electrons and ions with SuperDARN observations of ionospheric irregularities and convection for 2000–2100 MLT.

located at $\Lambda = 56°$ and successfully detected the boundary at 1550 UT and 1724 UT. Here the association of high-energy fluxes of participating particles with higher-velocity flows is less obvious, but the discrepancies may be a consequence of the inability of the radars to detect the lowest-latitude irregularities. Again in this sector, all precipitation is located equatorward of the CRB.

[19] Finally, in Figure 5 we compare eight DMSP overpasses in the postdawn sector (0600–0900 MLT) with SuperDARN observations of ionospheric irregularities and convection. In the dawn convection cell, electron precipitation is expected to extend to lower latitudes than ion precipitation. Therefore, we have ordered the data in terms of increasing activity as determined by the low-latitude boundary of electron precipitation as observed by DMSP. The level of geomagnetic activity for these events ranged from quiet to rather disturbed. For the two most disturbed cases (1312 UT and 1454 UT), the precipitation extended to $\Lambda = 60°$. This is 2° equatorward of the lowest latitude that the relevant radars (Kapuskasing and Saskatoon in central Canada) make observations. Figure 5 shows that dawn sector precipitation is also located equatorward of the CRB and associated with sunward convecting irregularities. Both the precipitation and the irregularities expand equatorward under more disturbed geomagnetic conditions.

[20] For the less disturbed cases in this time sector, there are indications that higher precipitating energy fluxes are associated with regions of higher-velocity convection. The two most disturbed cases do not support this conclusion, but it is likely that this is due to the inability of the radars to observe the full extent of the irregularity regions at that time. The results, in general, are consistent with the dusk-side results and strongly suggest that the data-sparse dawn-side convection cell shown in Figure 2 was probably more expanded than indicated in that figure.

4. Discussion

[21] In this paper, we have examined the mesoscale spatial relationship between precipitating electrons and ions observed with the DMSP spacecraft and radar backscatter observed with SuperDARN. The comparisons have been limited to the local time sectors spanning dawn and dusk, because of the local time distributions of the DMSP orbits. We have found that both quantities are best specified in terms of their relationship to the high-latitude convection pattern as derived by the SuperDARN observations. In

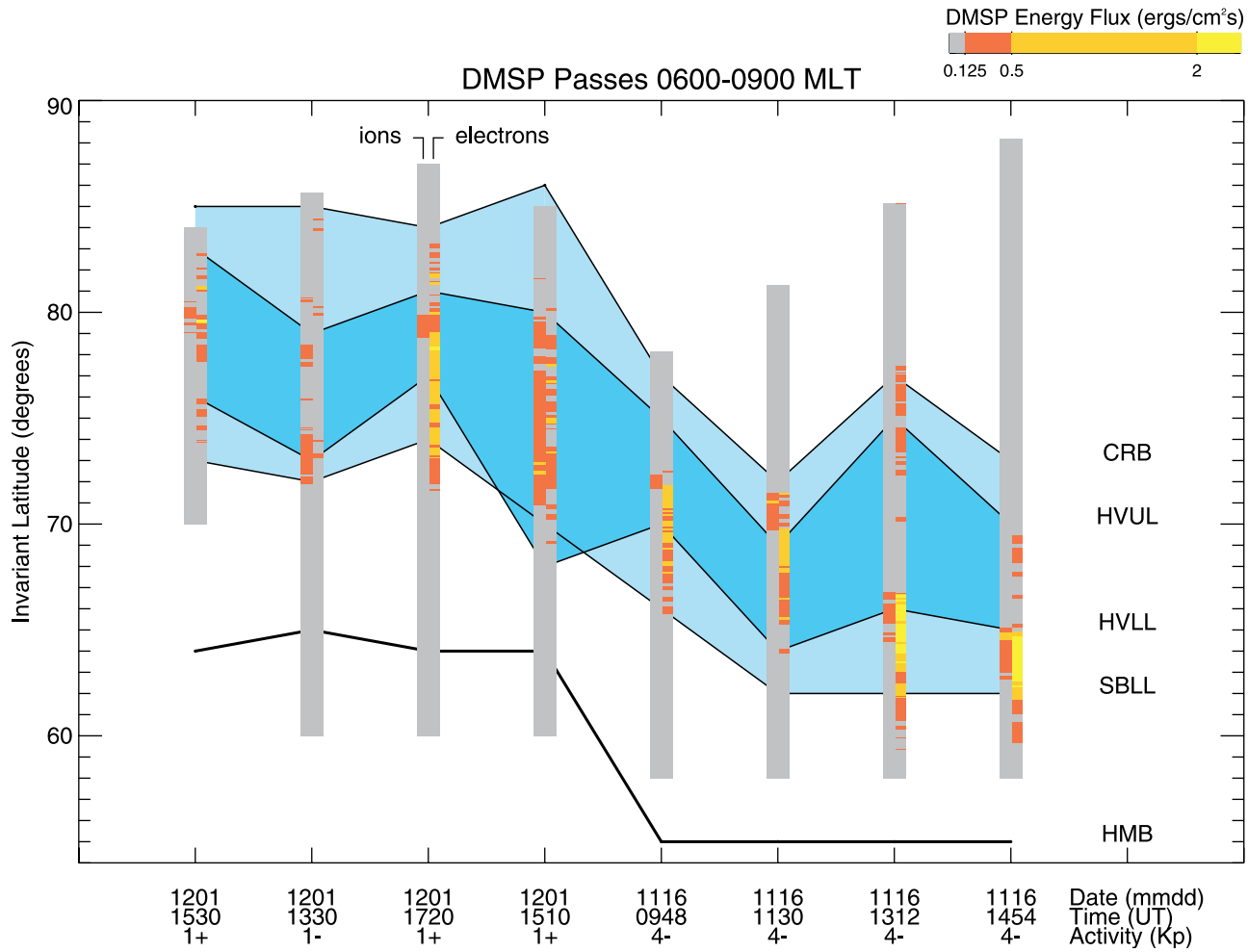

Figure 5. Comparison of DMSP observations of precipitating electrons and ions with SuperDARN observations of ionospheric irregularities and convection for 0600–0900 MLT.

general, ionospheric irregularities are observed over broad latitudinal regions extending from somewhat poleward of the Heppner-Maynard convection boundary through the CRB and into the polar cap. Particle precipitation, in contrast, is confined to a narrower region of sunward plasma convection. The equatorward boundary of the particle precipitation is generally poleward of the equatorward boundary of the irregularities. The poleward boundary of precipitation lies somewhat equatorward of the CRB. Both the irregularities and the precipitation expand equatorward and exhibit greater latitudinal extent as the level of geomagnetic disturbance increases. Exceptions to this spatial relationship are attributed to intervals when the irregularity boundary expanded equatorward of where the SuperDARN radars were able to make measurements. There is a tendency for precipitation regions with the highest energy flux to be associated with regions of higher velocity convection. This last relationship is more apparent if the most disturbed cases are removed from the comparison.

[22] The small-scale limit of the spatial correlation between particle precipitation and irregularities is determined by the spatial resolution of the SuperDARN measurements. While the DMSP spacecraft have an along-track spatial resolution of ~7 km, the SuperDARN radars have a range resolution of ~45 km and an azimuthal resolution determined by the antenna beam width (nominally 100 km at a range of 1500 km). This resolution is further degraded by the SuperDARN analysis process which filters the data onto a grid with dimensions of ~100 km × ~100 km. Thus, while the spatial correlation is excellent at 100 km scales sizes, it may not extend down to the width of the individual features identified in the precipitation measurements.

[23] The observed relationship between particle precipitation and sunward convecting irregularities can be understood in terms of the physics of magnetosphere-ionosphere coupling and ionospheric plasma instabilities. Convection electric fields in the magnetosphere map along nearly equipotential magnetic field lines into the high-latitude ionosphere producing large ionospheric fields and enhanced ionospheric convection. Birkeland currents flow between the magnetosphere and ionosphere where they are closed by horizontal currents driven by the mapped magnetospheric convection fields. Finally, the particles carrying the Birkeland currents may be accelerated at mid altitudes [see *Borovsky*, 1993] and precipitate into the ionosphere, where they produce conductance enhancements and electron density gradients. Various combinations of electric fields, density gradients, and field-aligned currents produce a

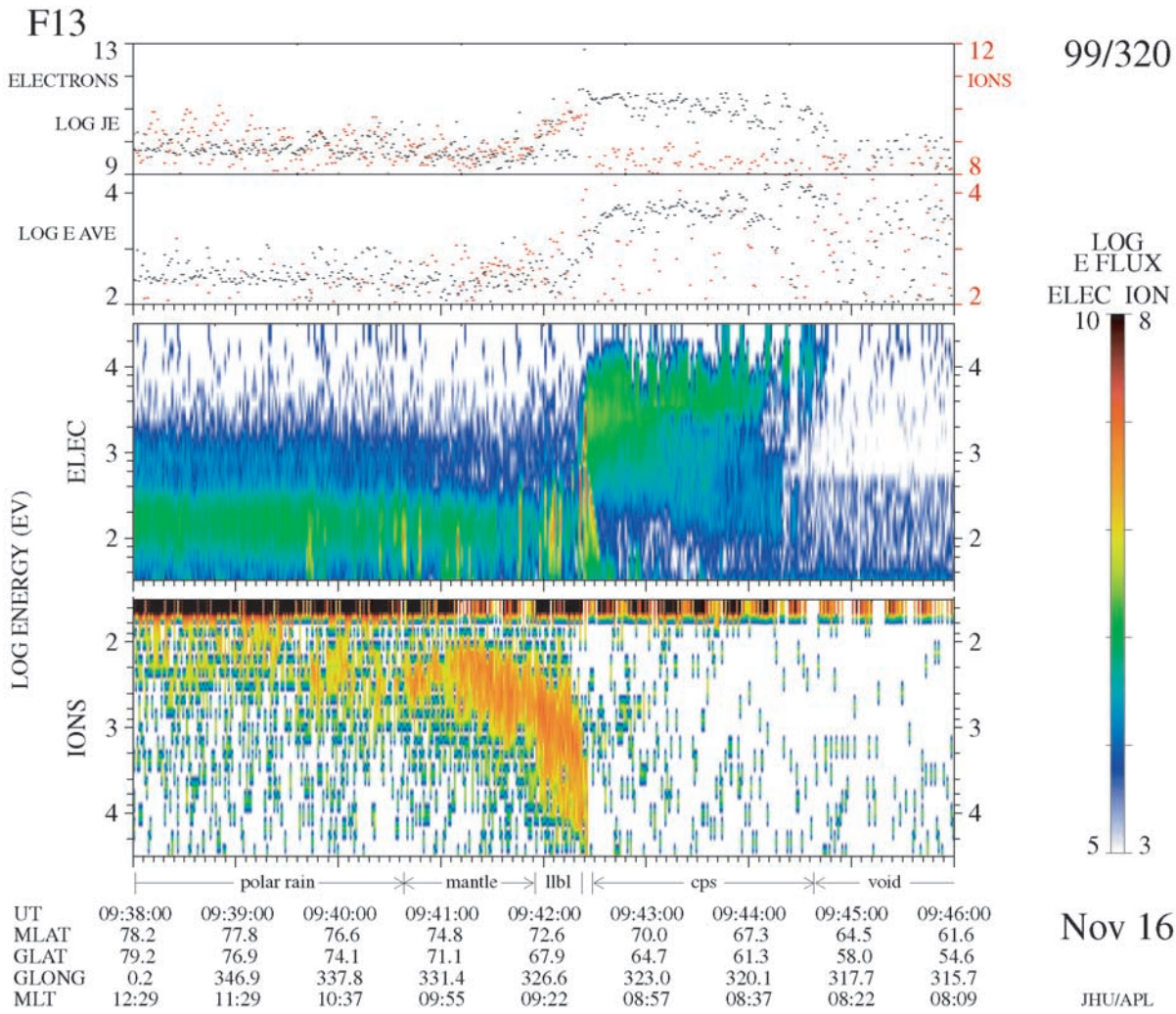

Figure 6. DMSP F13 observations from 16 November 1999 showing the passage of the satellite over the polar cap and into the post dawn auroral zone. The particle precipitation is identified as coming from the low-latitude boundary layer (LLBL) and the central plasma sheet (CPS).

broad range of low-frequency plasma instabilities in the ionosphere at both *E* region and *F* region altitudes. Some of the more notable of these include the *E* region two-stream [*Farley*, 1963; *Buneman*, 1963] and gradient drift instabilities [*Rogister and D'Angelo*, 1970], the *F* region gradient drift [*Reid*, 1968; *Keskinen et al.*, 1980], and current convective instabilities [*Ossakow and Chaturvedi*, 1979]. Electron density gradients, potentially produced by the precipitating particles, are an important source of free energy in many of these instabilities, as is the ionospheric electric field. The existence of these enhanced density gradients and electric fields are two reasons why there should be significant correlation between regions of ionospheric irregularities and zones of particle precipitation.

[24] On the other hand, some rocket experiments and radar studies have shown that there is often a strong negative correlation at smaller scale sizes between intense particle precipitation and large ionospheric electric fields [e.g., *Evans et al.*, 1977; *Cahill et al.*, 1978]. Ionospheric electric fields may be depressed as a consequence of mid-altitude acceleration processes causing V-type or S-type potential drops and leaving reduced electric fields in the underlying ionosphere [*Mozer et al.*, 1980]. In the presence of depressed ionospheric electric fields, some instability mechanisms may become inoperative. This is true, for example, of the *E* region two-stream instability [*Farley*, 1963; *Buneman*, 1963] and may also be true to some degree for the *E* region gradient drift instability. Enhanced *E* region conductances are also known to have a negative impact on the growth of *F* region instabilities [*Vickrey and Kelley*, 1982; Haerendel, personal communication, 2001]. Enhanced conductances allow stronger currents to flow across magnetic field lines and can lead to shorting of the electrostatic wave fields. The competition between destabilizing effects such as density gradients and large electric fields and stabilizing effects such as depressed electric fields and enhanced current flow across magnetic field lines makes it difficult to assess whether a particular

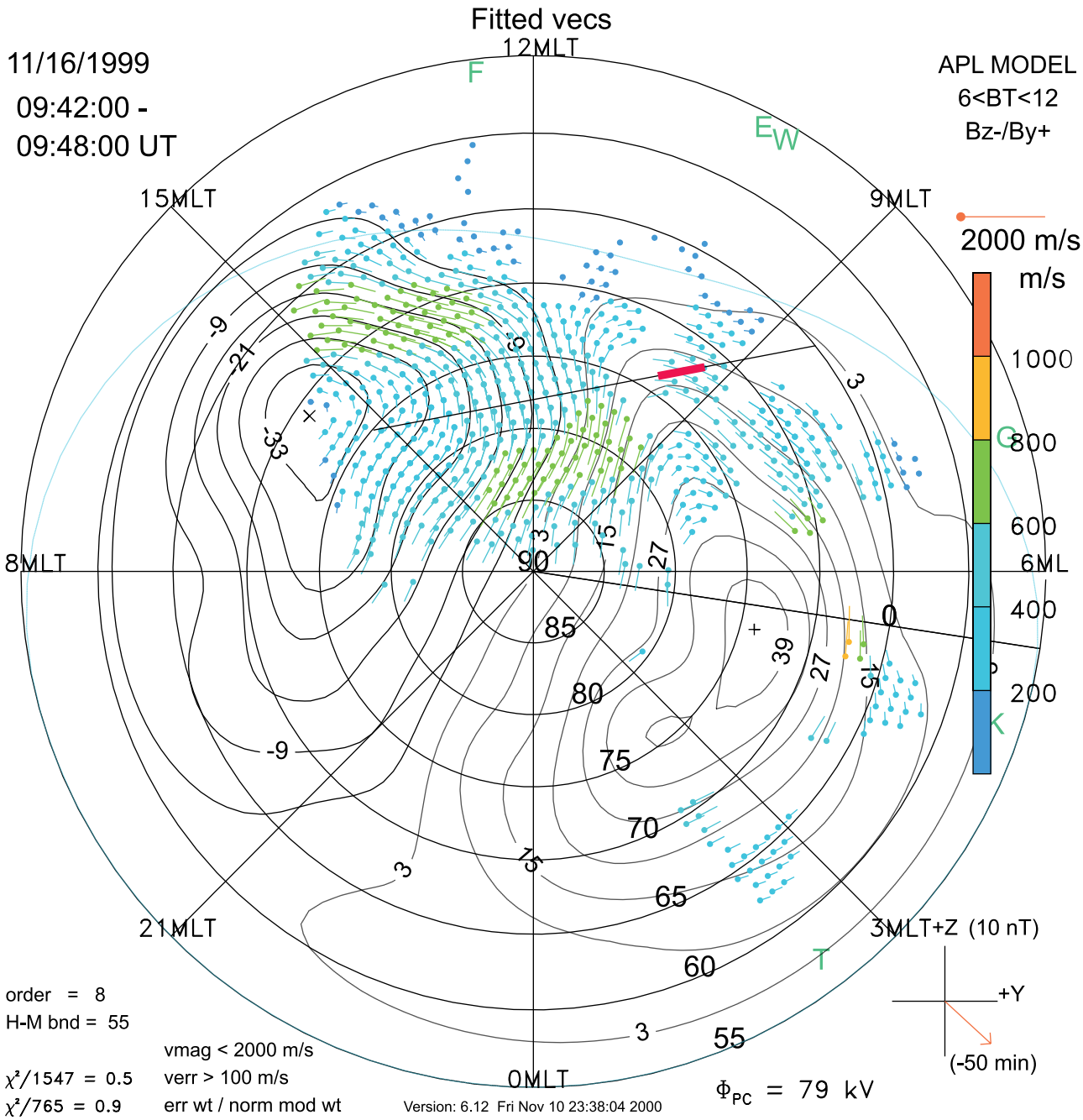

Figure 7. SuperDARN potential map showing high-latitude convection pattern at the time of the DMSP F13 crossing. The thin black line represents a portion of the footprint, while the heavier red segment represent the portion of the orbit in which LLBL precipitation was detected. The ionospheric convection is directed sunward and poleward, and is roughly antiparallel to the spacecraft trajectory in the LLBL. Poleward of the LLBL the spacecraft is on mantle field lines, and the flow becomes poleward and antisunward.

condition will lead to growth or decay of irregularities. Thus it is by no means obvious that spatially confined regions of strong particle precipitation should necessarily be collocated with regions of ionospheric irregularities. Some of these subtleties of this discussion become more apparent at dimensions approaching those of auroral structures. *E* region auroral radar studies have yielded a number of examples of irregularities being found on the edges of auroral features. [e.g., *Balsley et al.*, 1973; *Greenwald et al.*, 1973; *Hall et al.*, 1990]. The finer points of this discussion are below the spatial resolution afforded by this study and are therefore beyond the scope of this paper.

[25] One significant feature of our observations is that the zone of particle precipitation is consistently found to be equatorward of the CRB in the local time sectors near dawn and dusk. Closer to local noon, we still find the particle precipitation to be located equatorward of the CRB. In contrast, *Newell et al.* [1991] have reported that near

10 MLT, the CRB lies within the zone of low-latitude boundary layer (LLBL) precipitation. *Newell et al.* [1991] also surveyed various observations at both low and high altitudes that have been made over the years in relation to the LLBL and found that convection in this region is highly variable. Examples were presented showing sunward and antisunward convection as well as stagnation.

[26] We have examined the electron and ion precipitation spectra for the events identified in our study and found that, in most cases, the precipitation was on closed field lines and associated with the central plasma sheet (CPS) or boundary plasma sheet (BPS). However, in two events associated with the 0600–0900 MLT sector, the DMSP particle data showed clear evidence for LLBL precipitation. In both of these cases, ionospheric convection within the region of LLBL precipitation was both poleward and sunward. Thus, in both cases the LLBL was identified as being equatorward of the CRB.

[27] In Figure 6 we present the DMSP particle spectra for one of the LLBL detections. This pass is identified as 0948 UT on 16 November 1999 in Figure 5. Equatorward of $\Lambda = 71.5°$, the precipitation is primarily due to electrons from the CPS. Poleward of this latitude, there is ion precipitation from the LLBL and then lower-energy ion precipitation from the plasma mantle. The decreasing ion energy with increasing magnetic latitude is indicative of velocity dispersion effects in the precipitation of magnetosheath ions on open mantle field lines. There is also lower-energy bursty electron precipitation, most likely of magnetosheath origin, from the LLBL and mantle.

[28] Figure 7 displays the SuperDARN high-latitude convection pattern for the 6-min interval ending at 0948 UT. It was derived from Doppler data obtained from three successive radar scans. The convection cells are expanded at this time, commensurate with the disturbed geomagnetic conditions and a potential drop of 79 kV. A line representing the DMSP F13 trajectory is superposed on the convection pattern and the heavier red segment of the line is the location of the LLBL. The flow is roughly antiparallel to the satellite orbit in the LLBL and it exhibits both sunward and poleward flow components. The large number of velocity vectors plotted in the vicinity of the LLBL indicates that the convection was well determined in this region. Poleward of the LLBL, the spacecraft is on mantle field lines and the plasma convection exhibits initially poleward and then strongly antisunward flow.

[29] This example is very similar to the other event in which an LLBL signature was detected, but in that case the ion dispersion signature in the mantle was not as clearly observed. To summarize, for both cases where a LLBL signature was detected by DMSP, the convection was sunward and poleward in the ionosphere and sunward and toward the magnetopause boundary in the equatorial magnetosphere. Mantle field lines exhibited strongly antisunward flow.

[30] Our results show that *Bates et al.* [1973] was indeed correct when he postulated that radars could be used to detect the location of the auroral oval. The irregularity zone has somewhat greater latitudinal extent than the precipitation zone, but through the use of Doppler information it is possible to identify the portion that is associated with sunward convection. This segment is most closely associated with auroral precipitation under a wide range of geomagnetic conditions. While our results are directly applicable to the local time sectors near dawn and dusk, it seems reasonable that they should extend to other local times. This conjecture is based on the assumption that similar magnetosphere-ionosphere coupling processes and plasma instability processes occur at all local times.

[31] With the SuperDARN network, the detection of ionospheric irregularities and derivation of global-scale ionospheric convection patterns have been carried out continuously over extended local time sectors. Convection measurements are transferred via the Internet to a common location and made available to a broad community in near real time. These results suggest that additional potentially useful information on the global distribution of auroral precipitation may be derived from the SuperDARN measurements. The auroral-oval identifications would be indirect, spatially coarse ($\sim$100 km scale), and subject to limitations imposed by the fixed radar locations. Under disturbed conditions, the auroral oval could expand equatorward of many of the radar sites, making it impossible to detect the full latitudinal extent of the auroral precipitation. Nevertheless, measurements of this nature could be a valuable supplement to traditional auroral observations in regions or under conditions where the latter may not be available.

[32] **Acknowledgments.** This work was funded by NSF grant ATM-9812078 and NASA grant NAG5-8361. Operations at the Northern Hemisphere SuperDARN radar sites are funded by the U.S. National Science Foundation (Goose Bay), NASA (Kapuskasing), the Canadian Natural Sciences and Engineering Research Council (Saskatoon), the French Institut National des Sciences de l'Univers (Stokkseyri), and the British Particle Physics and Astronomy Research Council (Pykkvibaer and Hankasalmi).

[33] Janet G. Luhmann thanks John R. Dudeney and Michael Keskinen for their assistance in evaluating this paper.

References

Balsley, B. B., W. L. Ecklund, and R. A. Greenwald, VHF Doppler spectra of radar echoes associated with a visual auroral form, Observations and implications, *J. Geophys. Res.*, *78*, 1681–1687, 1973.

Bates, H. F., S.-I. Akasofu, D. S. Kimball, and J. C. Hodges, First results from the north polar auroral radar, *J. Geophys. Res.*, *78*, 3857–3864, 1973.

Borovsky, J. E., Auroral arc thicknesses as predicted by various theories, *J. Geophys. Res.*, *98*, 6101–6138, 1993.

Buneman, O., Excitation of field aligned sound waves by electron streams, *Phys. Rev. Lett.*, *10*, 285–288, 1963.

Cahill, L. J., Jr., R. A. Greenwald, and E. Nielsen, Auroral radar and rocket double probe observations of the electric field across the Harang discontinuity, *Geophys. Res. Lett.*, *5*, 687–690, 1978.

Evans, D. S., N. C. Maynard, J. Troim, T. Jacobsen, and A. Egeland, Auroral vector electric field and particle comparisons, 2, Electrodynamics of an arc, *J. Geophys. Res.*, *82*, 2235–2249, 1977.

Farley, D. T., Two-stream plasma instability as a source of irregularities in the ionosphere, *Phys. Rev. Lett.*, *10*, 279–282, 1963.

Fejer, B. G., and M. C. Kelley, Ionospheric irregularities, *Rev. Geophys.*, *18*, 401–454, 1980.

Greenwald, R. A., W. L. Ecklund, and B. B. Balsley, Auroral currents, irregularities, and luminosity, *J. Geophys. Res.*, *78*, 8193–8203, 1973.

Greenwald, R. A., et al., DARN/SuperDARN: A global view of the dynamics of high-latitude convection, *Space Sci. Rev.*, *71*, 761–796, 1995.

Hall, G., D. R. Moorcroft, L. L. Cogger, and D. Andre, Spatial relationship between large aspect angle VHF radaio aurora and 557.7-nm emissions: Evidence for refraction, *J. Geophys. Res.*, *95*, 15,281–15,288, 1990.

Hanuise, C., J.-P. Villain, J. C. Cerisier, C. Senior, J. M. Ruohoniemi, R. A. Greenwald, and K. B. Baker, Statistical study of high-latitude *E*-region Doppler spectra obtained with the SHERPA HF radar, *Ann. Geophys.*, *9*, 273–285, 1981.

Heppner, J. P., and N. C. Maynard, Empirical high latitude electric field models, *J. Geophys. Res.*, *92*, 4467, 1987.

Keskinen, M. J., S. L. Ossakow, and B. E. McDonald, Nonlinear evolution of diffuse auroral *F* region ionospheric irregularities, *Geophys. Res. Lett.*, *7*, 573–576, 1980.

Kivanc, O., and R. A. Heelis, Spatial distribution of ionospheric plasma and field structures in the high-latitude *F* region, *J. Geophys. Res.*, *103*, 6955–6968, 1998.

Milan, S. E., T. K. Yeoman, M. Lester, E. C. Thomas, and T. B. Jones, Initial backscatter occurrence statistics from the CUTLASS HF radars, *Ann. Geophys.*, *15*, 703, 1997.

Mozer, F. S., C. A. Cattell, M. K. Hudson, R. L. Lysak, M. Temerin, and R. B. Torbert, Satellite measurements and theories of auroral acceleration mechanisms, *Space Sci. Rev.*, *27*, 155, 1980.

Newell, P. T., W. J. Burke, E. R. Sanchez, C.-I. Meng, M. E. Greespan, and C. R. Clauer, The low-latitude boundary layer and the boundary plasma sheet at low altitude: Prenoon precipitation regions and convection reversal boundaries, *J. Geophys. Res.*, *96*, 21,013–21,024, 1991.

Ossakow, S. L., and P. K. Chaturvedi, Current convective instability in the diffuse aurora, *Geophys. Res. Lett.*, *6*, 332–334, 1979.

Reid, G. C., The formation of small-scale irregularities in the ionosphere, *J. Geophys. Res.*, *73*, 1627–1640, 1968.

Rogister, A., and N. D'Angelo, Type II irregularities in the equatorial electrojet, *J. Geophys. Res.*, *75*, 3879, 1970.

Ruohoniemi, J. M., and K. B. Baker, Large-scale imaging of high-latitude convection with Super Dual Auroral Radar Network HF radar observations, *J. Geophys. Res.*, *103*, 20,797–20,811, 1998.

Ruohoniemi, J. M., and R. A. Greenwald, Rates of scattering occurrence in routine HF radar observations during solar cycle maximum, *Radio Sci.*, *32*, 1051–1070, 1997.

Shepherd, S. G., and J. M. Ruohoniemi, Electrostatic potential patterns in the high-latitude ionosphere constrained by SuperDARN measurements, *J. Geophys. Res.*, *105*, 23,005–23,014, 2000.

Vickrey, J. F., and M. C. Kelley, The effects of a conducting *E* layer on classical *F* region cross-field plasma diffusion, *J. Geophys. Res.*, *87*, 4461–4468, 1982.

R. J. Barnes, R. A. Greenwald, J. M. Ruohoniemi, and T. Sotirelis, Applied Physics Laboratory, Johns Hopkins University, Laurel, MD 20723-6099, USA. (robin.barnes@jhuapl.edu; ray.greenwald@jhuapl.edu; mike_ruohoniemi@jhuapl.edu; tom_sotirelis@jhuapl.edu)

S. G. Shepherd, Thayer School of Engineering, Dartmouth College, 8000 Cummings Hall, Hanover, NH 03755, USA. (simon.g.shepherd@dartmouth.edu)